UNIVERSITY OF LEEDS

This is a repository copy of *Ozone Production Underestimation Over the Tibetan Plateau: The Role of NOx and OVOCs Modeling Uncertainties*.

White Rose Research Online URL for this paper:
https://eprints.whiterose.ac.uk/227667/

Version: Accepted Version

Article:

Wang, J., Wang, H., Zhang, C. et al. (18 more authors) (2025) Ozone Production Underestimation Over the Tibetan Plateau: The Role of NOx and OVOCs Modeling Uncertainties. Journal of Geophysical Research: Atmospheres, 130 (10). e2025JD043321. ISSN 2169-897X

https://doi.org/10.1029/2025jd043321

This is an author produced version of an article published in Journal of Geophysical Research: Atmospheres, made available under the terms of the Creative Commons Attribution License (CC-BY), which permits unrestricted use, distribution and reproduction in any medium, provided the original work is properly cited.

Reuse
This article is distributed under the terms of the Creative Commons Attribution (CC BY) licence. This licence allows you to distribute, remix, tweak, and build upon the work, even commercially, as long as you credit the authors for the original work. More information and the full terms of the licence here:
https://creativecommons.org/licenses/

Takedown
If you consider content in White Rose Research Online to be in breach of UK law, please notify us by emailing eprints@whiterose.ac.uk including the URL of the record and the reason for the withdrawal request.

White Rose
university consortium
Universities of Leeds, Sheffield & York

eprints@whiterose.ac.uk
https://eprints.whiterose.ac.uk/

Ozone Production Underestimation over the Tibetan Plateau: The Role of NO_x and OVOCs Modeling Uncertainties

Jianshu Wang[1], Haoqi Wang[2], Chong Zhang[1], Yaru Wang[1†], Yingjie Zhang[1‡], Jiacheng Zhou[3], Wanyun Xu[4], Lisa K. Whalley[5], Joanna E. Dyson[5], Eloise J. Slater[5], Chengzhi Xing[6], Suzhen Chi[1], Yumingzi Wang[1], Lifan Wang[1], Xuena Yu[1], Limin Zeng[1], Weili Lin[7], Weixiong Zhao[4], Dwayne E. Heard[5], Shaojie Song[2], Chunxiang Ye[1*]

[1] State Key Joint Laboratory for Environmental Simulation and Pollution Control, College of Environmental Sciences and Engineering, Peking University, Beijing, 100871, China.

[2] State Environmental Protection Key Laboratory of Urban Ambient Air Particulate Matter Pollution Prevention and Control & Tianjin Key Laboratory of Urban Transport Emission Research, College of Environmental Science and Engineering, Nankai University, Tianjin, China.

[3] Laboratory of Atmospheric Physico-Chemistry, Hefei Institutes of Physical Science Anhui Institute of Optics and Fine Mechanics, Chinese Academy of Sciences, Hefei, 230031, Anhui, China.

[4] Chinese Academy of Meteorological Science, Institute of Atmospheric Composition, Beijing, 100081, China.

[5] School of Chemistry, University of Leeds, Leeds, LS2 9JT, UK.

[6] Key Lab of Environmental Optics & Technology, Anhui Institute of Optics and Fine Mechanics, Hefei Institutes of Physical Science, Chinese Academy of Sciences, Hefei 230031, China.

[7] Key Laboratory of Ecology and Environment in Minority Areas, Minzu University of China, National Ethnic Affairs Commission, Beijing 100081, China.

Corresponding author: Chunxiang Ye (c.ye@pku.edu.cn)

[†] Now at Atmospheric Chemistry Department, Leibniz Institute for Tropospheric Research (TROPOS), Leipzig 04318, Germany.

[‡] Now at School of Ecology and Nature Conservation, Beijing Forestry University, Beijing 100083, China.

Key Points:

- Field observations serve as benchmarks for evaluating uncertainties in GEOS-Chem's simulation of the O_3 chemical budget.
- GEOS-Chem underestimates O_3 chemical production by 60% compared to observations.
- Model biases in O_3 chemistry are largely driven by model underestimations of NO_x, with significant contributions from OVOCs.

Abstract

Chemical production and destruction are key components of the tropospheric ozone (O_3) budget, yet significant model spreads exist among various global models in estimating O_3 chemical budgets. Observations in the background atmospheres play a crucial role in validating and evaluating model uncertainties in O_3 chemistry. Here we conducted comprehensive observations of the O_3 chemical budget at a remote site on the Tibetan Plateau. By comparing the observed O_3 chemical budgets with those simulated by GEOS-Chem, a global chemical transport model, we identified a 60% underestimation in the O_3 production rate by GEOS-Chem. Detailed budget analysis of O_3 and radicals revealed that this discrepancy primarily arose from GEOS-Chem's inadequate representation of nitrogen oxides (NO_x), followed by oxygenated volatile organic compounds (OVOCs). Comparisons with previous studies indicate a widespread model bias in simulating O3 precursors and their chemical budgets. These findings underscore the challenges in understanding O_3 chemistry linked to our imperfect understanding of the atmospheric fate of NO_x and OVOCs.

Plain Language Summary

Tropospheric ozone (O_3) plays a crucial role in air quality, climate change, and ecosystem health. The estimate and prediction for tropospheric O_3 levels and variabilities are heavily dependent on our understanding of the O_3 chemical budgets. However, significant simulation spreads of tropospheric O_3 photochemistry exist among various chemical transport models, indicating an incomplete scientific understanding of O_3 chemistry. This study compares the observed O_3 chemical budget with predictions from the GEOS-Chem model, and analyzes the source of modeling uncertainties. A significant underestimation of O_3 chemical production by GEOS-Chem is derived, which is primarily due to uncertainties in simulating nitrogen oxides (NO_x) and oxygenated volatile organic compounds (OVOCs). Future efforts should particularly focus on refining the representation of NO_x and OVOCs to improve our understanding of O_3 chemistry and enhance predictive capabilities for O_3 changes and their environmental impacts.

Keywords

Tropospheric ozone, atmospheric photochemistry, reactive nitrogen, carbonyl compounds, chemical transport model

1 Introduction

Tropospheric ozone (O_3) stands as a critical factor influencing air quality, climate change, human health, and ecosystem productivity (*Monks et al.*, 2015). It plays a central role in the photochemical oxidation of air pollutants, directly reacting with alkenes and generating OH radicals, the key oxidant in the atmosphere, through photolysis (*Levy*, 1971). Ranked as the third-largest greenhouse gas after carbon dioxide and methane, tropospheric O_3 significantly influences the Earth's radiative balance, with a direct radiative forcing of ~0.4 W m^{-2} according to the sixth assessment report of IPCC (*Intergovernmental Panel on Climate Change*, 2023). In addition, O_3 exposure poses adverse effects on human health, agricultural yields, and ecosystem productivity (*Ainsworth et al.*, 2012; *Arjomandi et al.*, 2018). The significance drives a substantial interest among researchers and policymakers to understand the distribution and variability of tropospheric O_3.

The distribution and variability of tropospheric O_3 are determined by an interplay of several physical and chemical processes, known as O_3 budgets. Physical budgets of O_3 involve processes such as stratosphere-to-troposphere transport and surface deposition, while chemical budgets include chemical production via the oxidation reactions of precursors like nitrogen oxides ($NO_x = NO + NO_2$) and volatile organic compounds (VOCs) under ultraviolet light, alongside its chemical destruction through photolysis and reactions with radicals and alkenes. Chemical production and destruction constitute the major terms in the global tropospheric O_3 budget, estimated at ~5000 Tg yr^{-1} on average, significantly outweighing physical budget terms (*Young et al.*, 2018). Notably, regions with high surface O_3 concentration usually coincide with areas of elevated production rate of O_3, such as polluted regions. Moreover, the long-term trends of net O_3 production, i.e., O_3 chemical production minus its chemical destruction, closely align with the trends of O_3 concentration over the last decades (*Archibald et al.*, 2020), emphasizing the pivotal role of chemical budgets in shaping O_3 distribution and trends.

Despite incorporating the state-of-the-art understanding of O_3 chemistry, global models exhibit large spreads in simulating O_3 chemical budgets. As assessed in a recent model intercomparison project, the Atmospheric Chemistry-Climate Model Intercomparison Project (ACCMIP), models' estimates of O_3 chemical budgets vary by a factor of 2 (*Young et al.*, 2018). Additionally, chemistry-climate models have been found to underestimate O_3 change rates by over 50% over the past 5-6 decades (*Parrish et al.*, 2014). These model uncertainties indicate an incomplete understanding of the chemical processes, which hinders our ability to estimate the historic O_3 trends and predict its future changes and environmental impacts, including radiative forcing (*Iglesias-Suarez et al.*, 2018).

Efforts have been made to elucidate the sources of the uncertainties in O_3 chemistry simulations. Sensitivity analyses of global models have revealed a significant sensitivity of O_3 to its precursor emissions and various chemical factors such as mechanisms, kinetics, photolysis frequencies, and atmospheric humidity (*Christian et al.*, 2017; *Ridley et al.*, 2017; *Wild et al.*, 2020). The ACCMIP evaluation highlights that significant uncertainties stem from poor models' representation of the chemical and physical processes of O_3 and its precursors (*Young et al.*, 2018). Observations in the background atmosphere provide crucial constraints of tropospheric O_3 chemistry, which serve as benchmarks for model validation and evaluation, aiding in identifying the uncertainty sources in the model. For example, observation-to-model comparisons of O_3 chemistry in the tropical marine boundary layer have highlighted that the omission of halogen chemistry significantly contributes to modeling errors in O_3 chemical destruction (*Read et al.*, 2008). Aircraft measurements and subsequent comparisons to model results have uncovered consistent model underestimation of NO_x, the chemical precursor of O_3, in the troposphere by global models (*Nicely et al.*, 2016; *Ye et al.*, 2023). In remote forested regions, emissions of biogenic VOCs, notably isoprene, together with NO_x, are attributed to the discrepancies in the O_3 chemical budget and O_3 concentration between observations and chemical transport model predictions (*Pike et al.*, 2010).

The in-depth study of atmospheric chemistry over the Tibetan Plateau from spring to summer of 2019, referred to as the @Tibet 2019, offers an opportunity to comprehensively observe the O_3 chemical budget in the background atmosphere. As the third pole of the world, with an average altitude exceeding 4000m, the Tibetan Plateau represents the pristine tropospheric conditions. Our study presents the detailed O_3 chemical budget observations during the @Tibet 2019 field campaign and compares them with those derived from the global model

GEOS-Chem. We reveal an alarming modeling bias in O_3 production by GEOS-Chem, with a 60% underestimation of O_3 production rates compared to our observations. Modeling uncertainties in NO_x and oxygenated volatile organic compounds (OVOCs) emerge as major contributors to the underestimation, with our observations serving as a benchmark for model evaluation.

2 Methods

2.1 Measurements of O_3 chemistry

The @Tibet 2019 field campaign took place at the Nam Co Multisphere Observation and Research Station (NMC, 30°46.44′N, 90°59.31′E, 4730 m a.s.l.) from April 28 to July 10, 2019. Located on the southeastern shore of Nam Co Lake and approximately 15 km north of the Nyainqentanglha Mountains, the NMC represents a pristine alpine site. Limited local anthropogenic emissions primarily stemmed from sporadic cooking activities and vehicle use at the station. A comprehensive dataset on O_3 chemistry was collected from May 1 to May 21 during the @Tibet 2019 campaign.

O_3 measurements were conducted using a commercial UV photometric analyzer (49C, Thermo Electronics, USA) with a time resolution of 1 min (*Xu et al.*, 2023). The limit of detection for the O_3 analyzer is determined to be 1 ppbv, and the precision was 2% of the instrument response as evaluated by multiple calibrations during the campaign. The O_3 instrument was usually calibrated with an O_3 primary standard calibrator (49i-PS, Thermo Scientific, USA). A calibration range of 0-200 ppbv was applied to fully cover our measurement range of ambient O_3 concentration during the campaign.

NO_x was measured using a customized two-channel broadband cavity-enhanced absorption spectrometer (BBCEAS) as described in *Fang et al.,* (2017). For this study, the optical cavities were extended from 42cm to 1 meter to improve the instrument response sensitivity. Instrument performance was evaluated by supplying cylinder zero air (purity>0.99.999%) through the sampling line for 7 hours (Figure S1a). During this period, the instrument responses were 8.4±32.4 (1σ) pptv for channel one and -4.3±17.7 pptv for channel two, respectively (Figure S1b). The precision of the BBCEAS instrument for NO_2 was determined to be ±10 pptv. Allan deviation analysis indicated a detection limit (1σ) of 16 and 25 pptv for NO_2 in channel one and channel two, respectively, at a time resolution of 36 s (Figure S1c). In this study, 1-min NO_2 measurement data were collected, and 1-h averaged NO_2 measurements were shown and used as observational constraints for the chemical box model. Throughout the campaign, the BBCEAS uncertainty was determined to be 4%.

During the field measurements, ambient air was directly sampled into channel two for NO_2 measurements. For NO_x measurements, ambient air was mixed with O_3 (5 ppmv) for NO titration before being sampled into channel one. However, NO titration in channel one was unsuccessful due to an O_3 generator power failure. Therefore, only NO_2 measurements from channel two were used for further analysis.

Nonmethane VOCs (NMVOCs) and OVOCs were analyzed using an online gas chromatography system equipped with mass spectrometry and a flame ionization detector (GC-MS/FID, TH-PKU 300B, Wuhan Tianhong Instrument Co. Ltd, China). Ambient VOCs were concentrated in a cryogen-free pre-concentration system with a temperature of -150 °C before C2-C5 hydrocarbons were quantified by the flame ionization detector, while C5-C12 hydrocarbons, OVOCs, and halocarbons were quantified by the mass spectrometer (*Wang et al.*, 2014). The time resolution of the instrument was 1 h. Multipoint calibrations were performed at the beginning and the end of the campaign, and daily single-point calibrations at 2 ppbv were conducted throughout the campaign. Photochemical Assessment Monitoring Station (PAMS) standard mixture and TO-15 standard mixture (100 ppbv, Spectra Gases Inc., New Jersey, USA) were used as the calibration source. The instrument uncertainties were within ±10% for all calibrated species. The limit of detections for single VOC species were characterized to be 0.01 - 0.05 ppbv.

Measurements of other parameters related to O_3 chemistry were briefly described as follows. HONO levels were observed using a commercial LOng-Path Absorption Photometer (LOPAP-03, QUMA, Germany), based on wet chemical sampling and photometric detection techniques (*Heland et al.*, 2001; *Wang et al.*, 2023). The detection limit of the LOPAP was 5 pptv at a time resolution of 3min. Carbon monoxide (CO), methane(CH_4), and water vapor were measured using a commercial wavelength-scanned cavity ring-down spectroscopy (model G2401, PICARRO). Formaldehyde could not be detected by the GC-MS/FID instrument, so a commercial MAX-DOAS instrument was employed (*Xing et al.*, 2021). The MAX-DOAS instrument captured the vertical distribution of HCHO at altitudes of 0–4 km, and average formaldehyde concentration in the lowest level (0–100 m) was applied in this study. Photolysis frequencies were measured using a spectroradiometer (CCD-Spectrograph, Meteorologie Consult GmbH, Germany). Meteorological parameters, such as temperature and pressure, were measured by an automatic weather station. Refer to Table S1 for a comprehensive list of parameters described above.

2.2 GEOS-Chem model description

The GEOS-Chem (version 13.3.4, DOI: https://zenodo.org/record/7254256) was utilized to simulate the O_3 photochemistry of the @Tibet observation period (1 to 21 May 2019). The configuration of the GEOS-Chem model was briefly described as follows. The GEOS-Chem model was driven by meteorological data obtained from the Modern-Era Retrospective Analysis for Research and Applications, version 2 (MERRA-2), which was retrieved from the NASA Global Modeling and Assimilation Office (GMAO) at the Goddard Earth Observing System (GEOS) (*Gelaro et al.*, 2017). The MERRA-2 data has a horizontal resolution of 0.625°(longitude) × 0.5°(latitude) and was regrided to 5°(longitude) × 4° (latitude) for input into the global nested-grid simulation. The simulation over the East Asian region (60° – 120° E, 10° – 50 ° N) was operated at a higher resolution of 0.625°×0.5°. The vertical grid structure comprised 47 hybrid sigma/pressure levels spanning from the surface to the mesosphere, with the lowest layers about 100 m in height.

Emissions were calculated using the Harvard-NASA Emissions Component (HEMCO, version 3.2.2) (*Keller et al.*, 2014). Global anthropogenic emissions of SO_2, NO_x, NH_3, CO, VOCs, dust, primary organic carbon, and black carbon were obtained from the Community Emissions Data System (CEDS) (*Hoesly et al.*, 2018) and then overwritten over mainland China by the Multi-resolution Emission Inventory (MEIC) (*Li et al.*, 2017; *Zheng et al.*, 2018). Biogenic VOC emissions were based on the Model of Emissions of Gases and Aerosol from Nature version 2.1 (MEGAN2.1) framework (*Guenther et al.*, 2012). Soil NO_x emissions were calculated using the Berkeley-Dalhousie Soil NO_x Parameterization (BDSNP) scheme (*Hudman et al.*, 2012).

$NO_x + O_x + Br + Cl + I +$ aerosols chemical mechanisms in the troposphere (fullchem) were included in the GEOS-Chem simulation (*Jacob*, 2000; *Mao et al.*, 2013). Photolysis frequencies were calculated with the FAST-JX v7.0 photolysis mechanism(*Eastham et al.*, 2014; *Wild et al.*, 2000). As for O_3 production, the reactions of NO with HO_2 radicals and 78 RO_2 species were included. As for O_3 loss, the reaction of O_3 with OH radicals, O_3 with HO_2 radicals, the O^1D atom (the product of O_3 photolysis) with H_2O, and NO_2 with OH radicals were included.

O_3 chemical budgets from the NMC grid (centered at 31°N, 91.25°E, 557 hPa) modeled by GEOS-Chem were extracted from the model. Additionally, modeled concentrations for O_3 and its precursors during the same period as the field campaign were extracted, compared with observations, and utilized for box model constraints for examination of chemical mechanisms related to O_3 chemistry in the GEOS-Chem. See Table S2 for a list of the parameters extracted from the GEOS-Chem.

2.3 Chemical box model description

A photochemical box model, based on the Framework for 0-D Atmospheric Modeling (F0AM, v4.0) (*Wolfe et al.*, 2016), was employed to calculate the chemical budget of O_3 and investigate the factors contributing to the bias in O_3 chemistry modeling. The chemical mechanisms of the box model were based on the Master Chemical Mechanism (MCM, v3.3.1), with a subset extracted from the MCM website (https://mcm.york.ac.uk/MCM/), comprising 11152 gas-phase reactions relevant to our VOC and OVOC measurement (*Jenkin et al.*, 2015; *Saunders et al.*, 2003). Gas-phase reaction rate constants were determined using equations from the MCM and constrained by our temperature and pressure observations. The photolysis frequencies were calculated using the parameterization method provided by the MCM (Eq. 1), which accounted for the solar zenith angles (*SZA*) based on the location of the site and the period of the campaign, and the species-specific coefficients (*l*, *m*, and *n*) extracted from the MCM website. Physical processes such as dilution and dry deposition were not incorporated into the chemical box model. The model timespan ranged from 1 to 21 May 2019, with a time step of 1h.

$$j = l \cdot \cos(SZA)^m \cdot \exp(-n \cdot \sec(SZA)) \qquad \text{Eq. 1}$$

In Eq.1, *j* represented the photolysis frequency; *SZA* represented the solar zenith angles; *l*, *m*, and *n* were species-specific coefficients.

Several model runs were designed to examine the O_3 chemistry and its influencing factors. The setup and configuration for each model run were described as follows.

A base model (referred to as Box_S0) was established to calculate the chemical budgets of O_3 constrained by our measurements. In the model, time series data for the parameters outlined in Table S1 were constrained with a time resolution of 1h. Due to a lack of NO measurements, simulation of NO was conducted in the model of Obs. where VOCs, NO_2, O_3, and HONO, along with the photolysis frequencies for NO_2 (j_{NO2}) and HONO (j_{HONO}) were constrained. Concentrations of radicals (OH, HO_2, and RO_2) were also predicted. Comparisons between the predictions of radicals and field observations were conducted to validate the model. As shown in Figure S2, the averaged measurement/model ratio of 0.88, 0.99, and 1.22 for OH, HO_2, and RO_2, respectively. The discrepancy between model prediction and observation of radical concentrations fell within the measurement uncertainty of ±25%. These evaluations validated the model's satisfactory representation of O_3 chemistry observation.

A GEOS-Chem model scenario (referred to as Box_GC) was designed to simulate the O_3 photochemistry constrained by GEOS-Chem extractions with the MCM chemical mechanism. All parameters listed in Table S2 were constrained in Box_GC with a time resolution of 1h. Compared with Obs. constraints, Box_GC was constrained with fewer NMVOCs and OVOCs species. The NMVOCs and OVOCs species extracted from the GEOS-Chem accounted for 80% of total OH reactivity and further contributed substantially to O_3 chemistry, while the species not extracted contributed little, as estimated by Box_GC. Moreover, the concentrations of the remaining NMVOCs and OVOCs species were nearly null as simulated in GEOS-Chem.

Sensitivity model runs (referred to as Box S1-S3) were designed to investigate the magnitude of O_3 chemistry change in response to its influencing factors and quantify the contribution of influencing factors to the modeling bias. The influencing factors included NMVOCs, OVOCs, and NO_x. Influencing parameters were substituted with measurements in the sensitivity model runs to serve as constraints, replacing the GEOS-Chem extractions. Specifically, in model S2, NMVOCs were constrained with our measurements in place of that extracted from GEOS-Chem, while other settings remained identical to model S1. In model S3, OVOCs were constrained with our measurements in place of those extracted from GEOS-Chem, while other settings remained identical to model S2. The measured concentration of NO_2 and modeled NO in model S0 was constrained in place of the NO_x extracted from GEOS-Chem in model S4, while other settings remained identical to model S3. By replacing and adding the measurement constraints of the influencing parameters instead of replacing them individually, the synthesized effects of these factors on O_3 chemistry were derived, considering that the factors were chemically coupled with each other.

For each model run described above, the O_3 production rate (P_{O3}) and the O_3 destruction rate (D_{O3}) were extracted from the model according to the equations below. Finally, the net chemical production rate of O_3 (Net_{O3}) is calculated by subtracting D_{O3} from P_{O3}.

$$P_{O3} = k_1[NO][HO_2] + \sum k_i[NO][RO_2]_i \qquad \text{Eq. 2}$$

$$D_{O3} = f \times j_{O^1D}[O_3] + k_2[O_3][HO_2] + k_3[O_3][OH] + k_4[NO_2][OH] \qquad \text{Eq. 3}$$

$$Net_{O3} = P_{O3} - D_{O3} \qquad \text{Eq.4}$$

In the equation above, the [*X*] represented the concentration of species *X*; j_{O^1D} was the photolysis frequency of O_3; f was the fraction of O^1D radicals reacting with H_2O to produce OH radical, relative to the total sink strength of O^1D radicals, which was calculated with H_2O concentration, temperature, and pressure.

3 Results and Discussion

3.1 Meteorological and chemical conditions

The time series of the meteorological and chemical parameters observed during the campaign are shown in Figure S3. Throughout the campaign, temperature varied from -6.4 °C to 13.7 °C with an average of 3.1±3.8(1σ) °C. Precipitations rarely occur during the campaign, limited to three small snow events. Wind patterns showed distinct diurnal cycles, with westerly winds reaching speeds of ~4-7 m s^{-1} in the daytime, shifting to the southerly winds accompanied by lower speeds at night. Solar radiation was notably intense, with j_{O^1D} reaching approximately 5.5×10^{-5} s^{-1} at noon, twice the level observed at the same latitude at the sea level (*Yang et al.*, 2021). These meteorological observations align with previous multi-year data from this site (*Yin et al.*, 2017), indicating stable and representative late-spring conditions on the plateau, characterized by cold and dry weather influenced by high altitude and westerlies.

The background nature of this site is further supported by observations of emission tracers. For instance, observed NO_2 concentrations averaged at 153±115(1σ) pptv. NO levels, calculated with Box_S0, averaged at 20±28(1σ) pptv, reaching ~50 pptv in the daytime (Figure S3d). CO and CH_4 were on the levels of 115±17(1σ) ppbv and 1.89±0.02(1σ) ppmv, respectively. Alkanes contributed the most to the NMVOC concentrations with a mean concentration of 2.67±0.65(1σ) ppbv (Figure S3f). The mixing ratios of NO_x and NMVOCs are similar to those measured at Waliguan global atmospheric watch station on the Tibetan Plateau (*Xue et al.*, 2013). Occasional spikes in NO_2 and NMVOC concentrations indicated the limited influence of anthropogenic emissions at the NMC station, such as cooking and vehicle emissions (Figure S3d&g). The biogenic sources were also relatively weak, with concentrations of alkenes on the order of 0.2 ppbv. It was worth noting that substantial levels of OVOCs were observed at this background site, with a mean value of 3.02±1.15(1sd) ppbv, primarily composed of formaldehyde, acetaldehyde, and acetone (Figure S3h).

Overall, observations of the meteorological and chemical parameters confirm the alpine background nature of the NMC site, characterized by minimal anthropogenic and biogenic emissions, representing the regional background atmospheric condition of the Tibetan Plateau. The meteorological and chemical conditions at NMC are comparable to those reported at other remote sites across the Tibetan Plateau, which indicate a stable and regionally representative atmospheric condition during our campaign. This makes NMC observations a suitable basis for model evaluation and comparison, even at the relatively coarse resolution of 0.5 degrees in the GEOS-Chem.

The observed O_3 concentration averaged at 61±14(1σ) ppbv, displaying a distinct bridge-shaped diurnal pattern. O_3 levels measured are in accordance with previous multi-year O_3 measurements at this site, which reported a concentration of 58.6±12.2(1σ) ppbv in May (*Yin et al.*, 2017). The O_3 levels are comparable with those measured at other remote sites over the Tibetan Plateau, such as the Waliguan Global Atmospheric Watch Station (*Xu et al.*, 2016), but higher than typical alpine background sites in the midlatitudes of the Northern Hemisphere, such as Jungfraujoch and Hohenpeissenberg (*Parrish et al.*, 2021; *Parrish et al.*, 2014). Compared to GEOS-Chem simulations, the observed O_3 concentrations were reasonably compared, especially during the daytime. Nevertheless, the GEOS-Chem failed to reproduce the distinct diurnal patterns observed (Figure S4). Previous research has shown that vertical mixing and downward transport of stratospheric and free-tropospheric air are the primary contributors to the enhanced O_3 concentration in the daytime over the Tibetan Plateau (*Xu et al.*, 2018; *Xu et al.*, 2023). GEOS-Chem's underestimation of the impact of deep stratospheric ozone intrusions at such high-altitude sites could partially explain the discrepancies in O_3 (*Fiore et al.*, 2014; *Zhang et al.*, 2020). Additionally, uncertainties in chemical budget terms also play a crucial role in influencing O_3 modeling accuracy (*Archibald et al.*, 2020). However, such discussions and comparisons remain limited due to the scarcity of observational constraints of O_3 chemistry, especially in remote atmospheres. In this study, the comprehensive suite of observational parameters regarding O_3 chemistry allowed for the detailed calculation and analysis of the O_3 chemical budget at Nam Co, enabling the model comparison and analysis of modeling uncertainties.

3.2 GEOS-Chem's underestimation of observed ozone chemical budget

The diurnal pattern of the O_3 chemical budget is shown in Figure 1a. Generally, P_{O3} exceeded the D_{O3} during daytime hours (8:00-20:00, Beijing Time), resulting in net O_3 chemical production. The average daytime P_{O3} and D_{O3} were at 0.8±0.3(1σ) and 0.4±0.2(1σ), respectively. The average daytime Net_{O3} reached 0.4±0.2(1σ) ppbv h^{-1}, with an accumulative Net_{O3} averaging at 3.5±3.2(1σ) ppbv day^{-1} over the campaign period. The net ozone production result aligns with the conclusions drawn from other continental background sites, and the Net_{O3} derived in this study is comparable with previous measurements (*Fischer et al.*, 2003; *Xue et al.*, 2013; *Zanis et al.*, 2000). For instance, at Waliguan, spring and summer daytime Net_{O3} were reported as 0.31 and 0.26 ppbv h^{-1}, respectively (*Xue et al.*, 2013). Net_{O3} was in the range of 0.1 to 0.3 ppbv h^{-1} at Mt. Cimone in summer (*Fischer et al.*, 2003), and in the range of 0.13 to 0.27 ppbv h^{-1} at the Mt. Jungfraujoch in spring and summer (*Zanis et al.*, 2000).

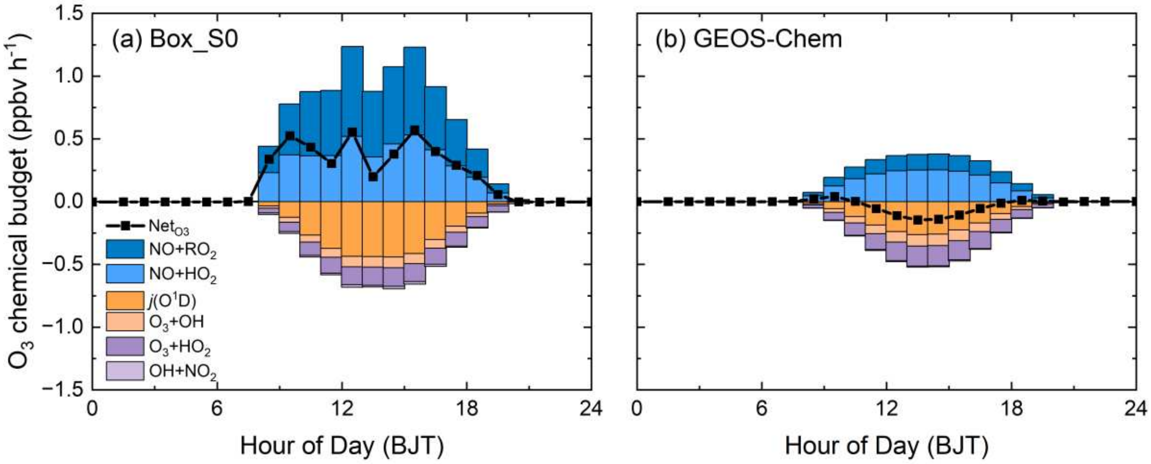

Figure 1. Diel pattern of O_3 chemical budget as calculated from (a) the box model constrained with observations at Nam Co (Box_S0) and (b) the GEOS-Chem model. In both panels, the light blue and dark blue bars represent the reaction rate of NO with HO_2 radicals and RO_2 radicals, respectively. The dark orange bars represent the reaction rate of the O^1D atom, the product of O_3 photolysis, with water vapor. The light orange bars represent the reaction rate of O_3 with OH radicals. The dark purple bars represent the reaction rate of O_3 with HO_2 radicals, and the purple bars represent the reaction rate of NO_2 with OH radicals, which competes with NO_2 photolysis and is considered an O_3 destruction pathway. The line shows the net O_3 production rate over the diel cycle.

In contrast to the Box_S0 simulation, the GEOS-Chem model predicted net O_3 chemical destruction in the daytime (Figure 1b). The average daytime Net_{O3} simulated by the GEOS-Chem was -0.05±0.06(1σ) ppbv h^{-1}. The P_{O3} simulated by GEOS-Chem was approximately 0.3±0.1(1σ) ppbv h^{-1} during the daytime, representing a 60% underestimation compared to observations. The D_{O3} was predicted at 0.3±0.2(1σ) ppbv h^{-1} in GEOS-Chem, which was slightly underestimated (~25%) relative to observations. As for specific terms in the O_3 chemical budget, reactions of NO with RO_2 and HO_2 radicals are both notably higher in the observations than in the GEOS-Chem simulation. For O_3 destruction, GEOS-Chem remarkably underestimated the rate of O_3 photolysis, while destruction budget terms were similar between observations and GEOS-Chem simulations.

Our finding regarding the significant underestimation of P_{O3} in global model simulations are consistent with results from previous research. For instance, in the marine troposphere, global model underestimation of O_3 precursors has been validated through comparisons with aircraft and satellite measurements, which result in similar biases in P_{O3} (*Nicely et al.*, 2016; *Shah et al.*, 2023). Similarly, studies over polar snowpacks have reported a 50% underestimation of NO_x by global models such as GEOS-Chem, which would further lead to P_{O3} underestimation (*Huang et al.*, 2017). Both our study and these previous investigations focus on remote atmospheres, which are more representative of the tropospheric atmosphere than studies conducted in polluted regions. These comparisons suggest that the model biases in O_3 chemical budgets identified in these studies may reflect a broader, potentially global issue, underscoring the importance of further attribution of this problem.

3.3 Factors controlling the ozone production underestimation

The discrepancies underscore GEOS-Chem's limitations in accurately modeling the O_3 chemical budget. The modeling uncertainties may come from either the different treatments of chemical mechanisms regarding O_3 chemistry between the box model and the GEOS-Chem, or the GEOS-Chem's bias in predicting these O_3 precursors or chemical parameters such as photolysis frequencies. In this section, we aim to attribute the discrepancies in the ozone chemical budget and identify the major sources of the modeling bias.

To evaluate the treatment of chemical mechanisms related to O_3 chemistry in GEOS-Chem, the GEOS-Chem modeled O_3 chemical budget was compared with a box model simulation constrained with GEOS-Chem extractions (Box_GC, Method). The box model was incorporated with the near-explicit chemical mechanism, Master Chemical Mechanism, and was validated to be reasonably satisfying for the radicals and thus O_3 chemical budget modeling at this remote site (Figure S2). The O_3 chemical budget simulated by Box_GC is shown in Figure S6. The average daytime P_{O3} and D_{O3} was 0.3±0.1(1σ) and 0.3±0.2(1σ) pptv h^{-1}, respectively, resulting the daytime Net_{O3} of -0.02±0.06(1σ). P_{O3}, D_{O3}, and Net_{O3} simulated by Box_GC were therefore comparable to GEOS-Chem model (Figure S6), excluding the treatment of chemical mechanism in the GEOS-Chem as the major reason for the observation to model discrepancies in O_3 chemical budget.

Simulation of O_3 precursor by GEOS-Chem was investigated and compared with our observations at Nam Co to further attribute the observation to model discrepancies. In background atmospheres, O_3 chemical production was strongly NO_x-limited, with NO reacting with peroxy radicals outcompeting the self-reaction of peroxy radicals, thereby resulting in O_3 chemical production (*Kleinman et al.*, 2001). We first compared the NO_x concentrations simulated by GEOS-Chem with observations at NMC and found an average underestimation of NO_x concentrations by 35% in GEOS-Chem (Figure 2a). As for diurnal patterns, GEOS-Chem underpredicted NO_x concentrations all day, with severe underestimation during the daytime (Figure 2c), posing a severer influence on O_3 production. Given the linear sensitivity of O_3 chemical production to NO_x concentration, a 35% underestimation of NO_x would lead to P_{O3} of a similar magnitude. However, the 60% underestimation of P_{O3} derived from our comparison could not be fully explained by uncertainties in NO_x simulations. The GEOS-Chem model underpredicts the reaction rate of NO with RO_2 radicals and HO_2 radicals by 70% and 40%, respectively (Figure 1), suggesting a model underestimation of other O_3 precursors.

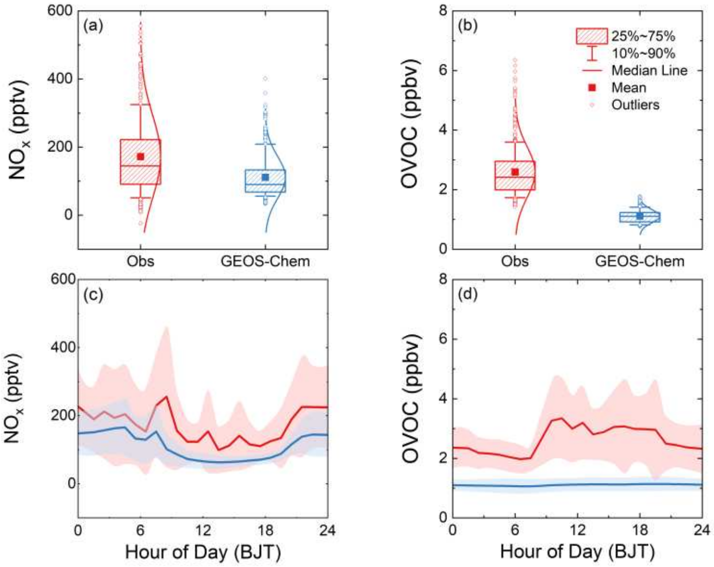

Figure 2. Comparison of the observation (red) with the GEOS-Chem simulation (blue) of O_3 precursors. Panels a-b compare the statistical distribution of NO_x and OVOC, respectively, and panels c-d compare the diurnal pattern of NO_x and OVOC, respectively. OVOC represents the sum concentration of formaldehyde, acetaldehyde, and acetone.

We then compared other O_3 precursors including NMVOCs, OVOCs, and CO between our observations and GEOS-Chem simulations. As shown in Figure 2b, GEOS-Chem underestimated OVOC concentrations by 60%. As for specific species, we found a 90% GEOS-Chem underestimation of acetaldehyde, followed by formaldehyde by 60% and acetone by 40% (Figure S2 & Figure S3). Moreover, the a larger discrepancy of OVOCs in the daytime than at nighttime. GEOS-Chem representation for NMVOCs seemed more accurate than OVOCs, with an underestimation of 40% (Figure S7b). In contrast, GEOS-Chem generally predicted the CO levels at Nam Co, with a discrepancy of 20% between simulations and observations (Figure S7a). A detailed budget of RO_x radicals (= OH, HO_2, and RO_2) was calculated using the Box_S0 model (box model constrained by our measurements) to examine the role of NMVOC and OVOCs in O_3 production. As shown in Figure S8, the reaction between OH radicals and OVOCs accounted for 40% of the total OH loss rate, leading to the production of RO_2 radicals, while the reaction between OH and NMVOCs contributed only around 10%. In addition to promoting secondary peroxy radical production via oxidation by OH radicals, photolysis of OVOCs directly generated HO_2 and RO_2 radicals, which contributed to 15% of the total RO_x radicals budget on the daytime average. Overall, our observations indicated that OVOCs greatly facilitated the primary production and chain propagation of radicals at this site, further promoting O_3 chemical production. Therefore, underestimation of OVOCs was deduced as another cause of P_{O3} underestimation in GEOS-Chem.

Other parameters influencing the O_3 production were also examined in this study. O_3 photolysis contributed to ~70% of RO_x radical sources (Figure S8) and further promoted O_3 chemical production. In addition, it presents as the major O_3 destruction pathway. Parameters affecting the O_3 photolysis rates, including O_3 concentration, photolysis frequency, and H_2O concentrations, were assessed. As shown in Figure S5&S7, GEOS-Chem overestimates O_3 concentrations by 15% on a daily average, while it overestimates daytime O_3 by about 7%. These discrepancies may reflect an underrepresentation of background O_3 levels and transport-chemistry interactions in the model. However, differences in O_3 concentrations cannot account for the 60% underestimation in O_3 chemical production compared to observations. j_{O1D} were reasonably represented in the model, with an observation-model discrepancy of 20%, which fell within the combined uncertainties of both measurements and modeling. A similar magnitude of underestimation, around 20%, was predicted for H_2O concentrations in the GEOS-Chem. These slight model discrepancies in O_3, j_{O1D}, and H_2O resulted in overall comparable O_3 photolysis rates between observations and GEOS-Chem simulations, with a minor discrepancy of around 25%.

Sensitivity model runs were conducted to examine the combined effects of NMVOCs, OVOCs, and NO_x on O_3 chemistry (Methods). The P_{O3}, D_{O3} and Net_{O3} calculated in each sensitivity model were compared with Box_S0 (box model scenario constrained with observations) and Box_GC (box model scenario constrained with GEOS-Chem extractions). In Box_S1, where observational constraints on NMVOCs were added, little change in P_{O3} was found, compared to Box_GC, and P_{O3} was still underestimated by the same magnitude (Figure 3). This could be explained by the limited contribution of NMVOCs to peroxy radical production and therefore O_3 chemistry (Figure S8). In contrast, since OVOCs contributed heavily to the peroxy radical production, adding observational constraints on OVOCs (Box_S2) leads to the P_{O3} underestimation decreased to 50% (Figure 3a) compared to Box_S0, and net O_3 production is predicted (Figure 3c). When observational constraints on NO_x were further added (Box_S3), P_{O3} underestimation decreased to 20% (Figure 3a). Comparing Box_S3 to Box_S0, P_{O3} and D_{O3} are underestimated by 20%, which could be explained by either the model-observation discrepancy between O_3, j_{O1D}, and water vapor as illustrated above. Overall, the sensitivity models revealed that NO_x simulation bias was the major contributor to the difference between GEOS-Chem predicted and observed O_3 chemical budgets, followed by OVOCs.

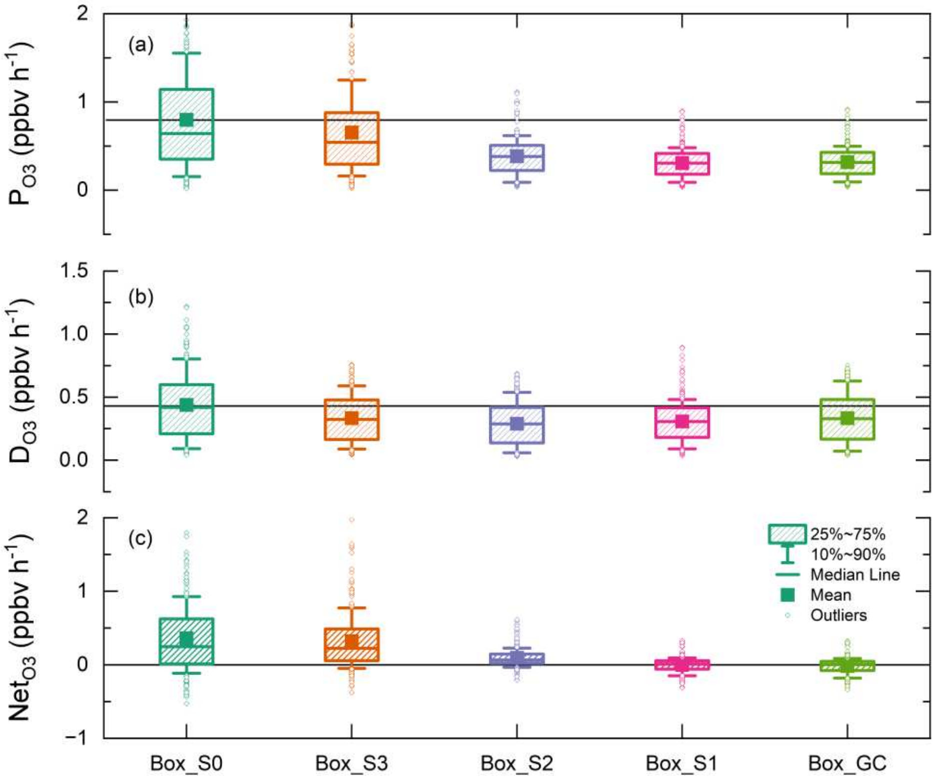

Figure 3. Daytime O_3 chemical budget calculated in each model scenario. (a) O_3 production rate (P_{O3}). (b) O_3 destruction rate (D_{O3}). (c) Net O_3 production rate (Net_{O3}). In each panel, Obs. represents the box model constrained with observations at Nam Co; Box_GC represents the box model constrained with GEOS-Chem model-extracted parameters related to O_3 chemistry; Box S1-S3 represent the sensitivity model run for NMVOCs (Box S1), OVOCs (Box S2), and NO_x (Box S3), respectively. The horizontal solid line in panels (a) and (b) represents the mean value of P_{O3} and D_{O3} in Obs., respectively. The horizontal solid line in panel (c) represents the zero net ozone chemical production.

Several factors may account for the model bias in NO_x and OVOCs, including poorly characterized emission inventories, incomplete model representation of their chemical and physical processes, such as inaccurate parameterization of soil-to-atmosphere exchange, and incomplete chemical mechanisms. Emission inventory handling was ruled out as the primary source of GEOS-Chem's underestimation of these O_3 precursors. Observations of low concentrations of anthropogenic and biogenic emission tracers confirm minimal local emissions at Nam Co, though emissions from upwind regions such as South Asia could potentially exert an influence. To investigate this, we conducted a sensitivity analysis by setting the NO_x emissions in South Asia to zero. As shown in Figure S9, this adjustment caused no significant change in NO_x output for the Nam Co grid. An underlying reason is that the reactive O_3 precursors are unlikely to survive the long-range transport from South Asia to the central Tibetan Plateau, compared to less reactive ones such as CO and water vapor (*Fu et al.*, 2006). These results indicate the model-to-observation discrepancies arose from something inherently wrong in the model, rather than simply a result of poorly characterized emissions.

The inaccurate soil emission parameterization scheme in the GEOS-Chem could be a possible reason for the model underestimation. Previous comparisons of soil NO_x emissions estimated by the BDSNP scheme and observations indicated the parametrization scheme tended to underestimate the soil NO_x emissions (*Lu et al.*, 2021). Soil emissions of HONO are another projected source of NO_x, which is not included in the current model scheme of soil emissions (*Hudman et al.*, 2012). Emitted HONO quickly photolyzes to produce NO_x via the internal cycle mechanism between HONO and NO_x in the atmosphere (*Wang et al.*, 2023). The comparison of modeled and observed HONO concentrations suggests GEOS-Chem underestimated HONO concentrations by around one order of magnitude (Figure S7 f), which supports missing HONO sources in GEOS-Chem such as soil emissions. As for OVOCs, missing emission sources from surface or plants might be attributed to the model bias of acetaldehyde and formaldehyde (*Travis et al.*, 2020; *Wang et al.*, 2019). In NMC observations, soil emission fluxes of formaldehyde were observed with distinct diurnal patterns following those in concentrations (not shown). Nevertheless, the OVOC emission included in GEOS-Chem for the Nam Co is negligible, which might account for the model underestimation of the OVOCs (*Guenther et al.*, 2012). For chemical mechanisms, omitting the photolysis of surface-absorbed nitrates also serves as a feasible reason for the NO_x underestimation in the GEOS-Chem (*Ye et al.*, 2023). Production from the photolysis of organic aerosols may provide a source for OVOCs (*Wang et al.*, 2019). Measurement constraints are necessary for optimizing these parameterizations and chemical mechanisms and their kinetics.

4 Conclusions and outlook

This study evaluated the simulation of O_3 chemical budgets in the GEOS-Chem model, using observations from a remote site on the Tibetan Plateau as a benchmark. Significant discrepancies were identified between observations and the GEOS-Chem simulations, with the model underestimating O_3 production rates by 60%. This model bias was primarily attributed to the inadequate representation of O_3 precursors in the models, rather than inaccuracies in chemical mechanisms regarding the O_3 production. Specifically, both NO_x and OVOCs were underestimated by GEOS-Chem, with biases ranging from 40% to 60%, consequently leading to the model underestimation of O_3 chemical production.

Model underestimations in NO_x and OVOCs have been widely reported across various background environments, including the marine troposphere and polar regions(*Huang et al.*, 2017; *Nicely et al.*, 2017; *Shah et al.*, 2023). Consistent with these studies, our results highlight that chemical transport models generally struggle to capture these O_3 precursors, which results in systematic biases in O_3 chemical production. These findings underscore the current knowledge gap in the understanding of the atmospheric fate of NO_x and OVOCs and their contributions to the tropospheric O_3 chemical budget. We hope this study motivates further observational constraints of the O_3 budget in remote regions, incorporating comprehensive budget closure analysis of reactive nitrogen and OVOCs.

Acknowledgments

The authors appreciate the assistance and contributions of all the researchers and staff involved in the @Tibet 2019 field campaign. This work was supported by the Ministry of Science and Technology of China (Grant No. 2022YFC3701104), Natural Science Foundation of Tianjin City

(Grant No. 22JCYBJC01330), and the National Natural Science Foundation of China (Grant No. 42375088). The authors declare no financial conflicts of interest.

Open Research

Observational data and model results used in this study are available at the Peking University Open Research Data website (*Wang*, 2024). F0AM box model framework and codes are available at (*Wolfe et al.*, 2016) and https://sites.google.com/site/wolfegm/models. MCM mechanisms are available via https://mcm.york.ac.uk/MCM/. The GEOS-Chem model used in this study is available via Zenodo (*Yantosca et al.*, 2022).

References

Ainsworth, E. A., C. R. Yendrek, S. Sitch, W. J. Collins, and L. D. Emberson (2012), The Effects of Tropospheric Ozone on Net Primary Productivity and Implications for Climate Change, in *Annual Review of Plant Biology, Vol 63*, edited by S. S. Merchant, pp. 637-661.

Archibald, A. T., J. L. Neu, Y. F. Elshorbany, O. R. Cooper, P. J. Young, H. Akiyoshi, et al. (2020), Tropospheric Ozone Assessment Report: A critical review of changes in the tropospheric ozone burden and budget from 1850 to 2100, *Elementa-Science of the Anthropocene*, *8*(1).doi:10.1525/elementa.2020.034.

Arjomandi, M., J. R. Balmes, M. W. Frampton, P. Bromberg, D. Q. Rich, P. Stark, et al. (2018), Respiratory Responses to Ozone Exposure MOSES (The Multicenter Ozone Study in Older Subjects), *American Journal of Respiratory and Critical Care Medicine*, *197*(10), 1319-1327.doi:10.1164/rccm.201708-1613OC.

Christian, K. E., W. H. Brune, and J. Q. Mao (2017), Global sensitivity analysis of the GEOS-Chem chemical transport model: ozone and hydrogen oxides during ARCTAS (2008), *Atmospheric Chemistry and Physics*, *17*(5), 3769-3784.doi:10.5194/acp-17-3769-2017.

Eastham, S. D., D. K. Weisenstein, and S. R. H. Barrett (2014), Development and evaluation of the unified tropospheric-stratospheric chemistry extension (UCX) for the global chemistry-transport model GEOS-Chem, *Atmospheric Environment*, *89*, 52-63.doi:10.1016/j.atmosenv.2014.02.001.

Fang, B., W. Zhao, X. Xu, J. Zhou, X. Ma, S. Wang, et al. (2017), Portable broadband cavity-enhanced spectrometer utilizing Kalman filtering: application to real-time, in situ monitoring of glyoxal and nitrogen dioxide, *Optics Express*, *25*(22), 26910-26922.doi:10.1364/OE.25.026910.

Fiore, A. M., J. T. Oberman, M. Y. Lin, L. Zhang, O. E. Clifton, D. J. Jacob, et al. (2014), Estimating North American background ozone in U.S. surface air with two independent global models: Variability, uncertainties, and recommendations, *Atmospheric Environment*, *96*, 284-300.doi:10.1016/j.atmosenv.2014.07.045.

Fischer, H., R. Kormann, T. Klüpfel, C. Gurk, R. K. Königstedt, U. Parchatka, et al. (2003), Ozone production and trace gas correlations during the June 2000 MINATROC intensive measurement campaign at Mt. Cimone, *Atmospheric Chemistry and Physics*, *3*, 725-738.doi:10.5194/acp-3-725-2003.

Fu, R., Y. Hu, J. S. Wright, J. H. Jiang, R. E. Dickinson, M. Chen, et al. (2006), Short circuit of water vapor and polluted air to the global stratosphere by convective transport over the Tibetan Plateau, *Proceedings of the National Academy of Sciences of the United States of America*, *103*(15), 5664-5669.doi:10.1073/pnas.0601584103.

Gelaro, R., W. McCarty, M. J. Suárez, R. Todling, A. Molod, L. Takacs, et al. (2017), The Modern-Era Retrospective Analysis for Research and Applications, Version 2 (MERRA-2), *Journal of Climate*, *30*(14), 5419-5454.doi:10.1175/jcli-d-16-0758.1.

Guenther, A. B., X. Jiang, C. L. Heald, T. Sakulyanontvittaya, T. Duhl, L. K. Emmons, and X. Wang (2012), The Model of Emissions of Gases and Aerosols from Nature version 2.1 (MEGAN2.1): an extended and updated framework for modeling biogenic emissions, *Geoscientific Model Development*, *5*(6), 1471-1492.doi:10.5194/gmd-5-1471-2012.

Heland, J., J. Kleffmann, R. Kurtenbach, and P. Wiesen (2001), A new instrument to measure gaseous nitrous acid (HONO) in the atmosphere, *Environmental Science & Technology*, *35*(15), 3207-3212.doi:10.1021/es000303t.

Hoesly, R. M., S. J. Smith, L. Y. Feng, Z. Klimont, G. Janssens-Maenhout, T. Pitkanen, et al. (2018), Historical (1750-2014) anthropogenic emissions of reactive gases and aerosols from the Community Emissions Data System (CEDS), *Geoscientific Model Development*, *11*(1), 369-408.doi:10.5194/gmd-11-369-2018.

Huang, Y. X., S. L. Wu, L. J. Kramer, D. Helmig, and R. E. Honrath (2017), Surface ozone and its precursors at Summit, Greenland: comparison between observations and model simulations, *Atmospheric Chemistry and Physics*, *17*(23), 14661-14674.doi:10.5194/acp-17-14661-2017.

Hudman, R. C., N. E. Moore, A. K. Mebust, R. V. Martin, A. R. Russell, L. C. Valin, and R. C. Cohen (2012), Steps towards a mechanistic model of global soil nitric oxide emissions: implementation and space based-constraints, *Atmospheric Chemistry and Physics*, *12*(16), 7779-7795.doi:10.5194/acp-12-7779-2012.

Iglesias-Suarez, F., D. E. Kinnison, A. Rap, A. C. Maycock, O. Wild, and P. J. Young (2018), Key drivers of ozone change and its radiative forcing over the 21st century, *Atmospheric Chemistry and Physics*, *18*(9), 6121-6139.doi:10.5194/acp-18-6121-2018.

Intergovernmental Panel on Climate Change, I. P. C. C. (2023), Climate Change 2022: Impacts, Adaptation, and Vulnerability. Contribution of Working Group II to the Sixth Assessment Report of the Intergovernmental Panel on Climate Change*Rep.*, Cambridge.

Jacob, D. J. (2000), Heterogeneous chemistry and tropospheric ozone, *Atmospheric Environment*, *34*(12-14), 2131-2159.doi:10.1016/s1352-2310(99)00462-8.

Jenkin, M. E., J. C. Young, and A. R. Rickard (2015), The MCM v3.3.1 degradation scheme for isoprene, *Atmospheric Chemistry and Physics*, *15*(20), 11433-11459.doi:10.5194/acp-15-11433-2015.

Keller, C. A., M. S. Long, R. M. Yantosca, A. M. Da Silva, S. Pawson, and D. J. Jacob (2014), HEMCO v1.0: a versatile, ESMF-compliant component for calculating emissions in atmospheric models, *Geoscientific Model Development*, *7*(4), 1409-1417.doi:10.5194/gmd-7-1409-2014.

Kleinman, L. I., P. H. Daum, Y. N. Lee, L. J. Nunnermacker, S. R. Springston, J. Weinstein-Lloyd, and J. Rudolph (2001), Sensitivity of ozone production rate to ozone precursors, *Geophysical Research Letters*, *28*(15), 2903-2906.doi:10.1029/2000gl012597.

Levy, H. (1971), Normal Atmosphere: Large Radical and Formaldehyde Concentrations Predicted, *Science*, *173*(3992), 141-143.doi:10.1126/science.173.3992.141.

Li, M., H. Liu, G. N. Geng, C. P. Hong, F. Liu, Y. Song, et al. (2017), Anthropogenic emission inventories in China: a review, *National Science Review*, *4*(6), 834-866.doi:10.1093/nsr/nwx150.

Lu, X., X. P. Ye, M. Zhou, Y. H. Zhao, H. J. Weng, H. Kong, et al. (2021), The underappreciated role of agricultural soil nitrogen oxide emissions in ozone pollution regulation in North China, *Nature Communications*, *12*(1).doi:10.1038/s41467-021-25147-9.

Mao, J. Q., F. Paulot, D. J. Jacob, R. C. Cohen, J. D. Crounse, P. O. Wennberg, et al. (2013), Ozone and organic nitrates over the eastern United States: Sensitivity to isoprene chemistry, *J. Geophys. Res.-Atmos.*, *118*(19), 11256-11268.doi:10.1002/jgrd.50817.

Monks, P. S., A. T. Archibald, A. Colette, O. Cooper, M. Coyle, R. Derwent, et al. (2015), Tropospheric ozone and its precursors from the urban to the global scale from air quality to short-lived climate forcer, *Atmospheric Chemistry and Physics*, *15*(15), 8889-8973.doi:10.5194/acp-15-8889-2015.

Nicely, J. M., R. J. Salawitch, T. Canty, D. C. Anderson, S. R. Arnold, M. P. Chipperfield, et al. (2017), Quantifying the causes of differences in tropospheric OH within global models, *J. Geophys. Res.-Atmos.*, *122*(3), 1983-2007.doi:10.1002/2016jd026239.

Nicely, J. M., D. C. Anderson, T. P. Canty, R. J. Salawitch, G. M. Wolfe, E. C. Apel, et al. (2016), An observationally constrained evaluation of the oxidative capacity in the tropical western Pacific troposphere, *J. Geophys. Res.-Atmos.*, *121*(12), 7461-7488.doi:10.1002/2016jd025067.

Parrish, D. D., R. G. Derwent, and J. Staehelin (2021), Long-term changes in northern mid-latitude tropospheric ozone concentrations: Synthesis of two recent analyses, *Atmospheric Environment*, *248*.doi:10.1016/j.atmosenv.2021.118227.

Parrish, D. D., J. F. Lamarque, V. Naik, L. Horowitz, D. T. Shindell, J. Staehelin, et al. (2014), Long-term changes in lower tropospheric baseline ozone concentrations: Comparing chemistry-climate models and observations at northern midlatitudes, *J. Geophys. Res.-Atmos.*, *119*(9), 5719-5736.doi:10.1002/2013jd021435.

Pike, R. C., J. D. Lee, P. J. Young, G. D. Carver, X. Yang, N. Warwick, et al. (2010), NOx and O-3 above a tropical rainforest: an analysis with a global and box model, *Atmospheric Chemistry and Physics*, *10*(21), 10607-10620.doi:10.5194/acp-10-10607-2010.

Read, K. A., A. S. Mahajan, L. J. Carpenter, M. J. Evans, B. V. Faria, D. E. Heard, et al. (2008), Extensive halogen-mediated ozone destruction over the tropical Atlantic Ocean, *Nature*, *453*(7199), 1232-1235.doi:10.1038/nature07035.

Ridley, D. A., M. Cain, J. Methven, and S. R. Arnold (2017), Sensitivity of tropospheric ozone to chemical kinetic uncertainties in air masses influenced by anthropogenic and biomass burning emissions, *Geophysical Research Letters*, *44*(14), 7472-7481.doi:10.1002/2017gl073802.

Saunders, S. M., M. E. Jenkin, R. G. Derwent, and M. J. Pilling (2003), Protocol for the development of the Master Chemical Mechanism, MCM v3 (Part A): tropospheric degradation of non-aromatic volatile organic compounds, *Atmospheric Chemistry and Physics*, *3*, 161-180.doi:DOI 10.5194/acp-3-161-2003.

Shah, V. R., D. J. Jacob, R. J. Dang, L. N. Lamsal, S. A. Strode, S. D. Steenrod, et al. (2023), Nitrogen oxides in the free troposphere: implications for tropospheric oxidants and the interpretation of satellite NO2 measurements, *Atmospheric Chemistry and Physics*, *23*(2), 1227-1257.doi:10.5194/acp-23-1227-2023.

Travis, K. R., C. L. Heald, H. M. Allen, E. C. Apel, S. R. Arnold, D. R. Blake, et al. (2020), Constraining remote oxidation capacity with ATom observations, *Atmospheric Chemistry and Physics*, *20*(13), 7753-7781.doi:10.5194/acp-20-7753-2020.

Wang, J., Y. Zhang, C. Zhang, Y. Wang, J. Zhou, L. Whalley, et al. (2023), Validating HONO as an Intermediate Tracer of the External Cycling of Reactive Nitrogen in the Background Atmosphere, *Environmental Science & Technology*, *57*(13), 5474-5484.doi:10.1021/acs.est.2c06731.

Wang, J. (2024), Nam Co Ozone Chemistry Dataset. [Dataset]. Peking University Open Research Data Platform, https://doi.org/10.18170/DVN/68OLNK.

Wang, M., L. M. Zeng, S. H. Lu, M. Shao, X. L. Liu, X. N. Yu, et al. (2014), Development and validation of a cryogen-free automatic gas chromatograph system (GC-MS/FID) for online measurements of volatile organic compounds, *Analytical Methods*, *6*(23), 9424-9434.doi:10.1039/c4ay01855a.

Wang, S. Y., R. S. Hornbrook, A. Hills, L. K. Emmons, S. Tilmes, J. F. Lamarque, et al. (2019), Atmospheric Acetaldehyde: Importance of Air-Sea Exchange and a Missing Source in the Remote Troposphere, *Geophysical Research Letters*, *46*(10), 5601-5613.doi:10.1029/2019gl082034.

Wild, O., X. Zhu, and M. J. Prather (2000), Fast-j: Accurate simulation of in- and below-cloud photolysis in tropospheric chemical models, *Journal of Atmospheric Chemistry*, *37*(3), 245-282.doi:10.1023/a:1006415919030.

Wild, O., A. Voulgarakis, F. O'Connor, J. F. Lamarque, E. M. Ryan, and L. Lee (2020), Global sensitivity analysis of chemistry-climate model budgets of tropospheric ozone and OH: exploring model diversity, *Atmospheric Chemistry and Physics*, *20*(7), 4047-4058.doi:10.5194/acp-20-4047-2020.

Wolfe, G. M., M. R. Marvin, S. J. Roberts, K. R. Travis, and J. Liao (2016), The Framework for 0-D Atmospheric Modeling (F0AM) v3.1, *Geoscientific Model Development*, *9*(9), 3309-3319.doi:10.5194/gmd-9-3309-2016.

Xing, C. Z., C. Liu, H. Y. Wu, J. A. Lin, F. Wang, S. T. Wang, and M. Gao (2021), Ground-based vertical profile observations of atmospheric composition on the Tibetan Plateau (2017-2019), *Earth System Science Data*, *13*(10), 4897-4912.doi:10.5194/essd-13-4897-2021.

Xu, W. Y., W. L. Lin, X. B. Xu, J. Tang, J. Q. Huang, H. Wu, and X. C. Zhang (2016), Long-term trends of surface ozone and its influencing factors at the Mt Waliguan GAW station, China - Part 1: Overall trends and characteristics, *Atmospheric Chemistry and Physics*, *16*(10), 6191-6205.doi:10.5194/acp-16-6191-2016.

Xu, W. Y., X. B. Xu, M. Y. Lin, W. L. Lin, D. Tarasick, J. Tang, et al. (2018), Long-term trends of surface ozone and its influencing factors at the Mt Waliguan GAW station, China - Part 2: The roles of anthropogenic emissions and climate variability, *Atmospheric Chemistry and Physics*, *18*(2), 773-798.doi:10.5194/acp-18-773-2018.

Xu, W. Y., Y. X. Bian, W. L. Lin, Y. J. Zhang, Y. R. Wang, Z. Q. Ma, et al. (2023), O₃ and PAN in southern Tibetan Plateau determined by distinct physical and chemical processes, *Atmospheric Chemistry and Physics*, *23*(13), 7635-7652.doi:10.5194/acp-23-7635-2023.

Xue, L. K., T. Wang, H. Guo, D. R. Blake, J. Tang, X. C. Zhang, et al. (2013), Sources and photochemistry of volatile organic compounds in the remote atmosphere of western China: results from the Mt. Waliguan Observatory, *Atmospheric Chemistry and Physics*, *13*(17), 8551-8567.doi:10.5194/acp-13-8551-2013.

Yang, X., K. Lu, X. Ma, Y. Liu, H. Wang, R. Hu, et al. (2021), Observations and modeling of OH and HO(2) radicals in Chengdu, China in summer 2019, *Science of the Total Environment*, *772*, 144829.doi:10.1016/j.scitotenv.2020.144829.

Yantosca, B., M. Sulprizio, L. Lundgren, kelvinhb, C. Keller, T. Fritz, et al. (2022). geoschem/geos-chem: GEOS-Chem 13.3.4 (13.3.4). [Software]. Zenodo. https://doi.org/10.5281/zenodo.7254256.

Ye, C. X., X. L. Zhou, Y. J. Zhang, Y. F. Wang, J. S. Wang, C. Zhang, et al. (2023), Synthesizing evidence for the external cycling of NO_x in high- to low-NO_x atmospheres, *Nature Communications*, *14*(1).doi:10.1038/s41467-023-43866-z.

Yin, X. F., S. C. Kang, B. de Foy, Z. Y. Cong, J. L. Luo, L. Zhang, et al. (2017), Surface ozone at Nam Co in the inland Tibetan Plateau: variation, synthesis comparison and regional representativeness, *Atmospheric Chemistry and Physics*, *17*(18), 11293-11311.doi:10.5194/acp-17-11293-2017.

Young, P. J., V. Naik, A. M. Fiore, A. Gaudel, J. Guo, M. Y. Lin, et al. (2018), Tropospheric Ozone Assessment Report: Assessment of global-scale model performance for global and regional ozone distributions, variability, and trends, *Elementa-Science of the Anthropocene*, *6*.doi:10.1525/elementa.265.

Zanis, P., P. S. Monks, E. Schuepbach, and S. A. Penkett (2000), The role of photochemistry in the control of ozone during spring at the Jungfraujoch (3,580 m asl) - Comparison of model results with measurements, *Journal of Atmospheric Chemistry*, *37*(1), 1-27.doi:10.1023/A:1006349926926.

Zhang, L., M. Y. Lin, A. O. Langford, L. W. Horowitz, C. J. Senff, E. Klovenski, et al. (2020), Characterizing sources of high surface ozone events in the southwestern US with intensive field measurements and two global models, *Atmospheric Chemistry and Physics*, *20*(17), 10379-10400.doi:10.5194/acp-20-10379-2020.

Zheng, B., D. Tong, M. Li, F. Liu, C. P. Hong, G. N. Geng, et al. (2018), Trends in China's anthropogenic emissions since 2010 as the consequence of clean air actions, *Atmospheric Chemistry and Physics*, *18*(19), 14095-14111.doi:10.5194/acp-18-14095-2018.

Figure 1.


(a) Box_S0
(b) GEOS-Chem
O_3 chemical budget (ppbv h^{-1})
1.5
1.0
0.5
0.0
−0.5
−1.0
−1.5
0
6
12
18
24
Hour of Day (BJT)
Net_{O3}
$NO+RO_2$
$NO+HO_2$
$j(O^1D)$
O_3+OH
O_3+HO_2
$OH+NO_2$

Figure 2.

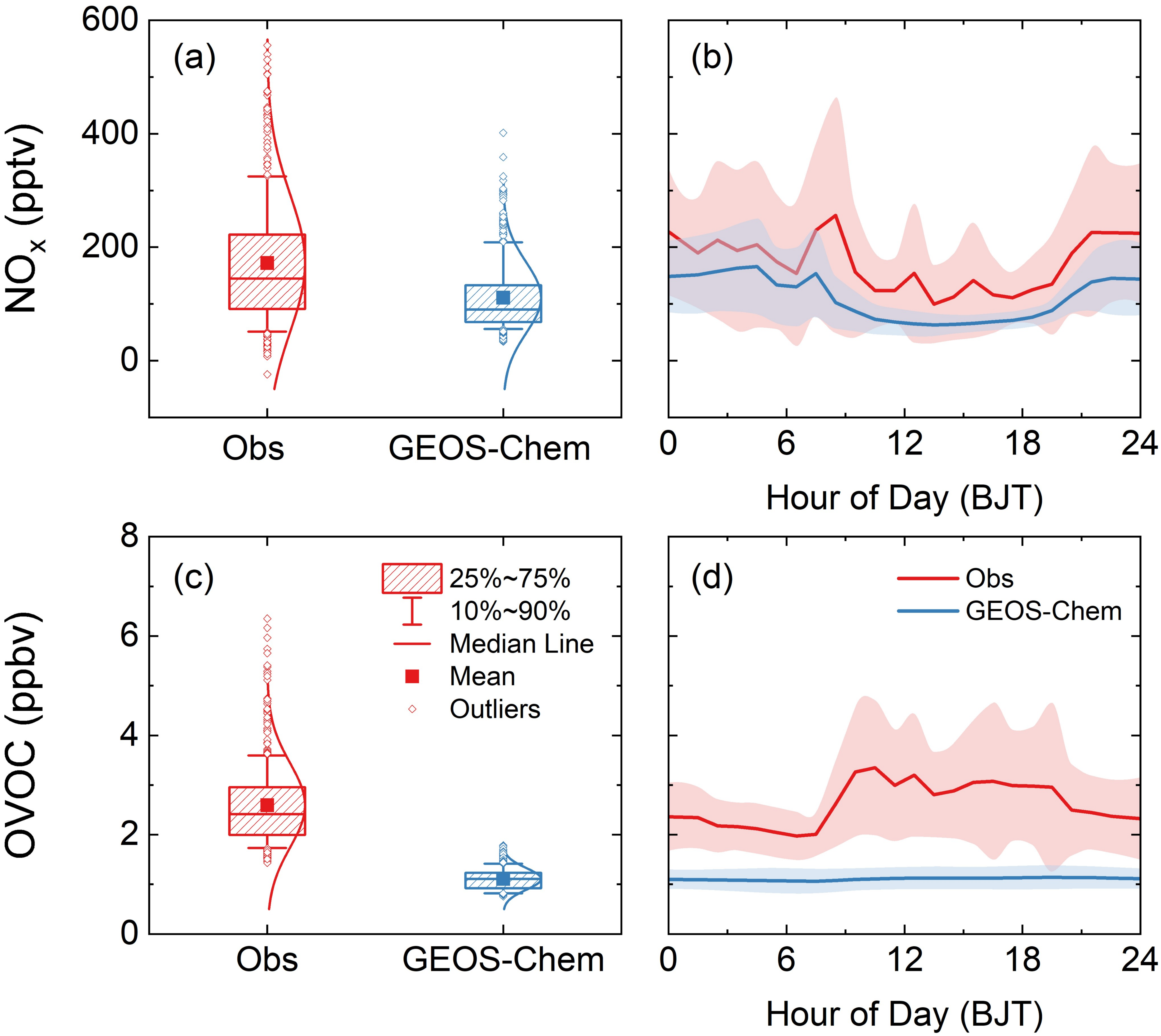
(a)
600
400
200
0
NO$_x$ (pptv)
Obs
GEOS-Chem
(b)
0
6
12
18
24
Hour of Day (BJT)
(c)
8
6
4
2
0
OVOC (ppbv)
25%~75%
10%~90%
Median Line
Mean
Outliers
Obs
GEOS-Chem
(d)
Obs
GEOS-Chem
0
6
12
18
24
Hour of Day (BJT)

Figure 3.

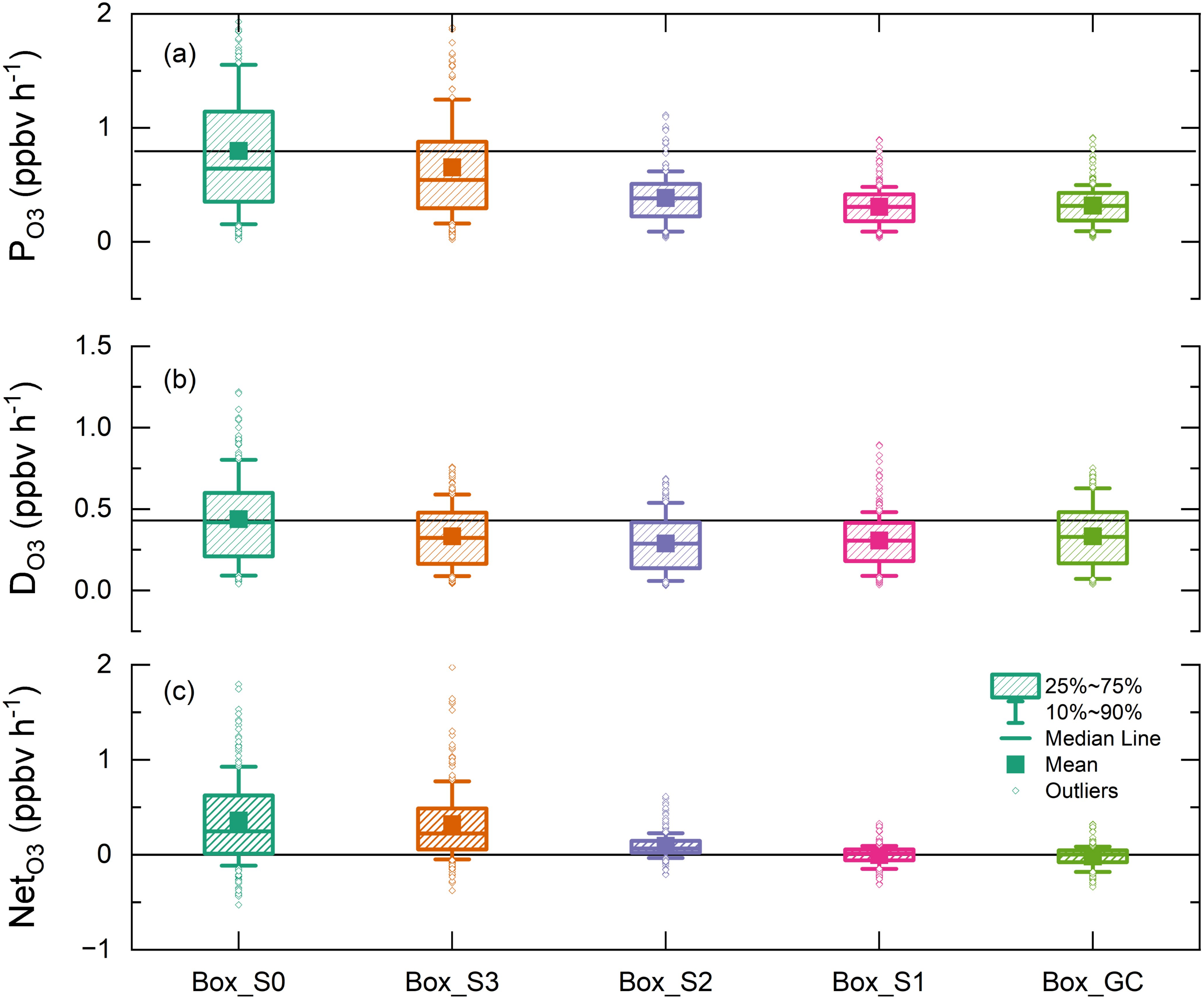
(a)
P_{O3} (ppbv h^{-1})
2
1
0
(b)
D_{O3} (ppbv h^{-1})
1.5
1.0
0.5
0.0
(c)
Net_{O3} (ppbv h^{-1})
2
1
0
−1
25%~75%
10%~90%
Median Line
Mean
Outliers
Box_S0
Box_S3
Box_S2
Box_S1
Box_GC